

A climatology of mesoscale convective systems over Europe using satellite infrared imagery. II: Characteristics of European mesoscale convective systems

By C. MOREL* and S. SENESI

Météo-France, France

(Received 11 December 2000; revised 23 November 2001)

SUMMARY

An automated method for mesoscale convective system (MCS) identification and tracking (described in part I) is applied in order to derive a sound European MCS database using Meteosat infrared channel (IR10.8) images centred over Europe, the western Mediterranean and north Africa. The database covers five warm seasons, from April to September, for the years 1993 to 1997 and includes more than 6000 MCSs reaching at least an area of 10 000 km².

First results of the derived climatology of European MCSs are presented. They mainly address the MCS geographical location, general MCS characteristics (maximum extent, eccentricity, duration) and the diurnal cycle of the MCS.

MCSs are shown to be mainly continental, but some MCS triggering is observed during the second half of August and September over the western Mediterranean Sea. Furthermore, MCS triggering is strongly correlated with orography and local maxima of MCS triggering are observed near all mountain ranges. Regions near the Alps which favour MCS triggering are described in detail. The monthly distributions of occurrence of warm-season European MCSs are also presented.

Distributions of maximum extent, eccentricity, direction of propagation, life duration and triggering and dissipation times are also derived. On average, a theoretical 'typical European MCS' moves to the east-north-east, triggers near 3 p.m. Local Solar Time (LST), lasts around 5.5 hours and dissipates near 9 p.m. LST. It typically has an eccentricity at the time of maximum extent of 0.53.

The diurnal cycle is also studied and proved to be in phase with the diurnal radiative heating, except for around 20% of the MCSs.

A detailed analysis of the maximum-extent distribution shows that it can be fitted by a log-normal distribution which leads to an average value of the MCS maximum extent of around 9000 km². This approximation is statistically meaningful and it is independent of the choice to study only MCSs reaching at least 10 000 km².

Finally, a section of this article is devoted to indirect verifications of the discrimination method (see part I) for the whole geographical domain.

KEYWORDS: Discrimination Diurnal cycle METEOSAT infrared data Occurrence Satellite features Tracking Triggering

1. INTRODUCTION

Numerous climatologies of mesoscale convective systems (MCSs) have been presented in the last 20 years. They were mainly established by using satellite and radar images and address principally (i) warm-season MCSs occurring over a given region which is often the USA where severe weather due to MCSs is frequent, (ii) tropical Africa where convective activity is intense, and (iii) more recently various parts of Europe. Even if a global climatology of mesoscale convective complexes (MCCs)—see Maddox (1980) for the definition of MCCs—was sketched by Laing and Fritsch (1997), global climatologies of MCSs remain rare.

US climatologies of MCSs mainly deal with MCCs which are quasi-circular meso- α scale (length-scale l between 250 and 2500 km) convective systems often responsible for great damage over the USA. They are also frequent in other parts of the world, such as in South America (Velasco and Fritsch 1987), in Africa (Laing and Fritsch 1993a), in the western Pacific region (Miller and Fritsch 1991), and in India (Laing and Fritsch 1993b), while they are comparatively rare in Europe. According to Laing and Fritsch (1997), a global population of 400 MCCs occurs each year. Thanks to these

* Corresponding author: Direction de la Prévision, Météo-France, 42 Avenue G. Coriolis, 31057 Toulouse Cedex, France. e-mail: Christophe.Morel@meteo.fr

climatologies, it is concluded that MCCs are mainly nocturnal MCSs which last about 10 hours and have a mean cold cloud-shield area of 350 000 km². It has also been shown that MCCs principally occur over land or close to coasts, in the lee (relative to mean mid-level flow) of mountain ranges and near zones of outgoing long-wave radiation gradients. These studies also led to a better understanding of the environment which is likely to favour MCC development (e.g. Augustine and Howard 1991; Anderson and Arritt 1996), and to the characterization of their precipitation life cycle (e.g. Kane *et al.* 1987; McAnelly and Cotton 1989).

Although studies concerning US MCC climatologies are frequent, studies dealing with US climatologies of non-MCC MCSs remain scarce. This lack is perhaps due to the fact that midlatitude MCSs which do not match MCC criteria are not objectively defined from satellite imagery. The building of a database of such MCSs then requires manual intervention and remains a tedious and time-consuming task. Nevertheless, a climatology of all US MCSs exceeding 10 000 km² below a temperature threshold of -52 °C was derived by Augustine *et al.* (1989). This includes more than 1000 MCSs. The geographical distribution, seasonal variability, diurnal cycle and distributions of MCS area and duration were examined. In particular, these authors showed that most of the MCSs do not satisfy the MCC criteria and that there is no gap in the distributions of maximum extent and duration. Results concerning the life cycle of MCSs were obtained using the same database (Tollerud *et al.* 1992).

Besides these US MCS climatologies, climatologies of tropical African MCSs often include all kinds of MCSs. Indeed, the building of an MCS database over tropical regions is easier than over midlatitude zones because most of the cold cloud shields of mesoscale dimensions are due to convective systems only. Consequently, the issue of an objective discrimination of MCSs is not instrumental over these regions and the tracking of MCSs remains the only problem to solve. A wide set of climatologies of tropical African MCSs exists at the present time and displays the general characteristics of MCSs, such as the maximum extent, duration, eccentricity, diurnal cycle, trajectories and occurrence charts (e.g. Arnaud *et al.* 1992; Machado *et al.* 1992; Mathon and Laurent 2001); the relationship between MCS development and environmental conditions is also presented in Hodges and Thorncroft (1997) using European Centre for Medium-range Weather Forecasts re-analyses.

For Europe, the realization of a sound MCS climatology based upon satellite imagery remains a hard task. Indeed, Europe is a midlatitude region so that objective discrimination of MCSs is required to automatically build an MCS database. Moreover, unlike in the USA, there are very few MCCs, consequently, European MCSs need to be defined using other criteria. Carretero and Riosalido (1996) computed a climatology of MCSs occurring over Spain. Distributions of size and duration, trajectories and occurrence charts, and the time evolution of the area at different temperature thresholds are presented for 67 MCSs exceeding 10 000 km². European MCS climatologies which are built from a database of satellite characteristics of several hundred MCSs do not seem to exist, so that the need for a sound European MCS climatology is real and should lead to a better knowledge of these systems. Thanks to the Instrument de Suivi dans l'Imagerie Satellitaire (ISIS) automated MCS tracking and discrimination method (see part I, Morel and Senesi 2002), it is now possible to derive such a climatology.

In this part of the two-part study, first results obtained over a five-year-long European MCS database are presented. The data used are Meteosat infrared images with a 30-minute time resolution and about a 6 km × 6 km spatial resolution on a polar stereographic grid. The geographical domain (see Fig. 1) covers western Europe, the western Mediterranean Sea and northern Africa. Section 2 addresses the counting of

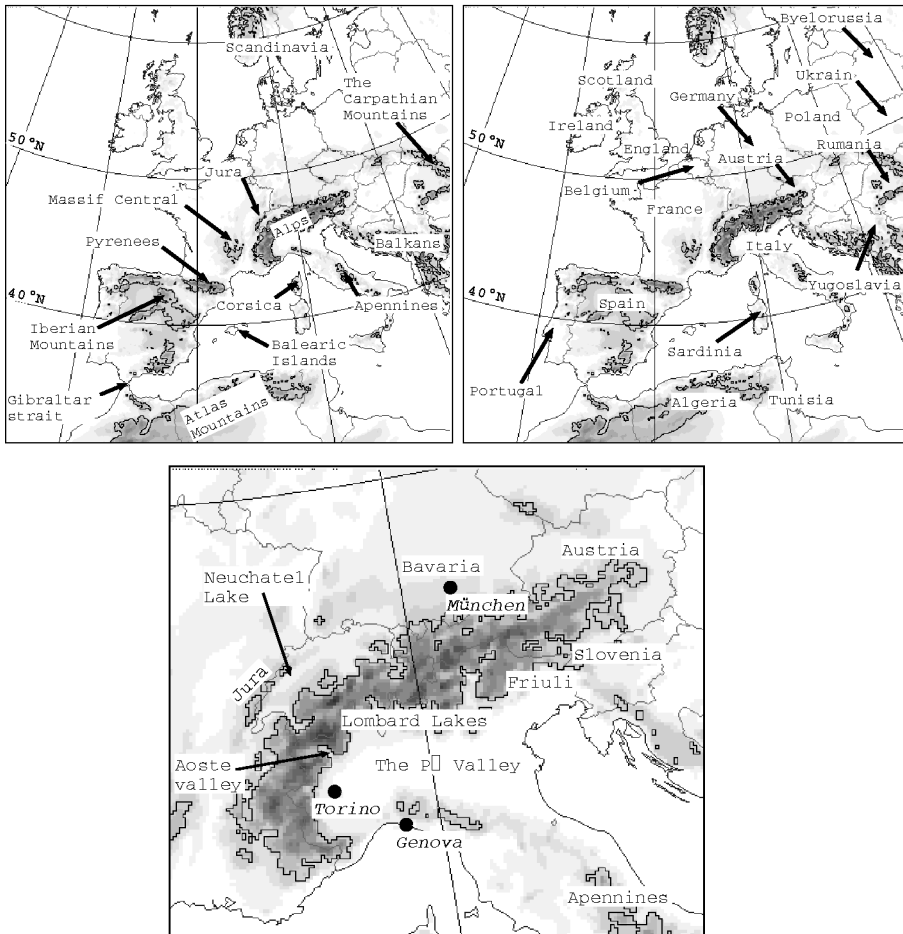


Figure 1. Geographical domain of the infrared images used for the current study with locations referred to in the text. The black solid line shows the 1000-metre elevation contour.

the MCSs and raises the issue of the ‘complexity’ of MCS trajectories. In section 3, maps of triggering and occurrence of European MCSs are presented. Sections 4 and 5, respectively, are devoted to morphological characteristics (maximum extent and eccentricity), duration and diurnal cycle. Finally, indirect verifications of the discrimination method, which is validated over France and surrounding areas but not over the whole geographical domain (see part I), are presented in section 6.

2. DESCRIPTIVE STATISTICS

In order to build the MCS database, the ISIS tracking method (see part I) was run over five warm seasons (from April to September for the years 1993 to 1997) at a temperature threshold $T_{th} = -45^{\circ}\text{C}$ and an area threshold $A_{th} = 1000\text{ km}^2$ (the geographical domain of the satellite images is displayed in Fig. 1). The derived MCS database is composed of all of the trajectories (6311 trajectories) satisfying the MCS discrimination criteria (see part I) and exceeding, at some stage, an area threshold $A_{min} = 10\,000\text{ km}^2$.

TABLE 1. NUMBER OF MESOSCALE-CONVECTIVE-SYSTEM TRAJECTORIES FOR EACH MONTH AND ACCORDING TO THE TYPE OF TRAJECTORY

Type	April	May	June	July	August	September	Total
Fully described	309	1010	1014	822	1066	471	4692
Interrupted by too many missing images	22	6	36	23	41	119	247
Interrupted by an edge of the domain	99	345	289	125	160	122	1140
<i>Over-crossing</i> trajectories	28	4	6	4	16	174	232
Total	458	1365	1345	974	1283	886	6311

Before running ISIS, a removal of noisy images (for instance, due to missing lines or to anomalous brightness temperatures) was undertaken to avoid failures in the tracking of cloud systems. After the removal of these noisy images, the available database of Meteosat infrared images was composed of 95% of the theoretically available images (only 89.9% in September because of the systematic gap of missing images during the equinoctial satellite eclipse periods).

The numbers of MCS trajectories included in the five-year-long database are given in Table 1 for each month and according to the type of trajectory (refer to the end of section 2(a) of part I):

- Interrupted by too many missing images.
- *Over-crossing* trajectories.
- Interrupted by an edge of the study area. For such a trajectory, at least one cell is cut by an edge of the domain.
- Fully described. These trajectories are the ‘normal’ trajectories for which (i) the tracking was not interrupted due to too many missing images and (ii) no cell was cut by an edge of the domain.

It is observed that 74.3% of MCS trajectories are fully described from the growth to the dissipation phase, and 4924 MCS trajectories (78%) are either fully described or *over-crossing* trajectories. As expected, *over-crossing* trajectories are numerous in September (20% of all the trajectories occurring in September) and stay marginal for the other months. Only 3.9% of trajectories are interrupted due to too many missing images showing the quality of the available infrared image database. Finally, around 18% of MCS trajectories are interrupted by an edge of the study area mainly because of the MCSs that trigger near the eastern border of the domain and develop eastward of this border. Also included are north-African MCSs which trigger southward of the southern edge of the domain and develop further inside the domain.

Concerning the seasonal cycle of convective activity, Table 1 shows that there is a large increase in convective systems between April and May (from 92 to 273 systems) when the warm season starts over Europe. Then, the monthly number of MCSs reaches a plateau from May to August and rapidly drops in September when the warm season ends. During months of maximum convective activity, the monthly number of trajectories is around 260 MCSs except for July, when the number of systems is around 195. This decrease is due to the combination in the database of two MCS populations, namely the European and north-African MCSs. It can be explained by the seasonal cycle of north-African MCSs and is no longer observed in the European MCS population (see section 3(c)).

Table 2 shows the number of MCS trajectories according to the type of the beginning and end of trajectory for the 4924 fully described or *over-crossing* MCS trajectories. The different kinds of beginnings or endings are:

TABLE 2. NUMBER OF MESOSCALE-CONVECTIVE-SYSTEM TRAJECTORIES ACCORDING TO THE TYPE OF BEGINNING AND ENDING

Beginning	End				Total
	Normal	Split	Merge	Complex	
Normal	2723	52	699	257	3731
Split	629	22	190	117	958
Complex	127	10	58	40	235
Total	3479	84	947	414	4924

TABLE 3. NUMBER OF INTEGRATED AND SPLIT CLOUD SYSTEMS ALONG THE TRAJECTORIES FOR THE *SIMPLE* MESOSCALE-CONVECTIVE-SYSTEM TRAJECTORIES SAMPLE

Integrated systems	Split systems				Total
	0	1	2	≥ 3	
0	373	250	109	47	779
1	188	255	178	126	747
2	54	113	111	174	452
≥ 3	12	49	90	594	745
Total	627	667	488	941	2723

- Split: beginning or end of the trajectory during a split of systems.
- Merge: end of the trajectory during a merge of systems.
- Complex: beginning or end of the trajectory during a ‘complex’ case.
- Normal: not after a split, or a merge or a ‘complex’ case (see part I, section 2(a) for the definition of these situations).

The main result is that MCS trajectories are rather complex and often interfere with other cloud-system trajectories. Indeed, only 3731 (76%) of the MCS trajectories start normally and around 55% (2723 trajectories) begin and end normally. Moreover, around 20% (958) of MCSs start after the split of a former cloud system and 20% (947) end by merging with another system. Consequently, isolated MCSs represent only around one half of the MCS population. Finally, another point is that the beginnings or endings during ‘complex’ situations exist but remain marginal (only 5% of the MCS trajectories start in a ‘complex’ case and 8% end that way).

Table 3 goes further in the analysis of MCS trajectory complexity. It displays the number of integrated and split cloud systems during the life of the 2723 MCSs which have a fully described or *over-crossing* trajectory with normal beginning and ending (hereafter this is called the *simple* MCS trajectories sample). It must be emphasized that the ‘relative weights’ of these integrated or split cloud systems are not taken into account. This means, for instance, that no distinction is made in the counting of integrated systems between the integrations of small and of large cloud systems.

Given this limitation, Table 3 emphasises the fact that isolated MCS trajectories are rare. Indeed, only 373 trajectories (14% of this sample and 7.5% of fully described or *over-crossing* MCS trajectories) begin and end normally and have neither merged nor split with other cloud systems during their life cycle. Besides, it shows that splits of cloud systems during an MCS life cycle are frequent and that around one third of MCSs split at least three times. It also shows that integrations of MCSs are less frequent than splits of systems. For instance, there are ‘only’ 745 (27%) MCS trajectories with three or

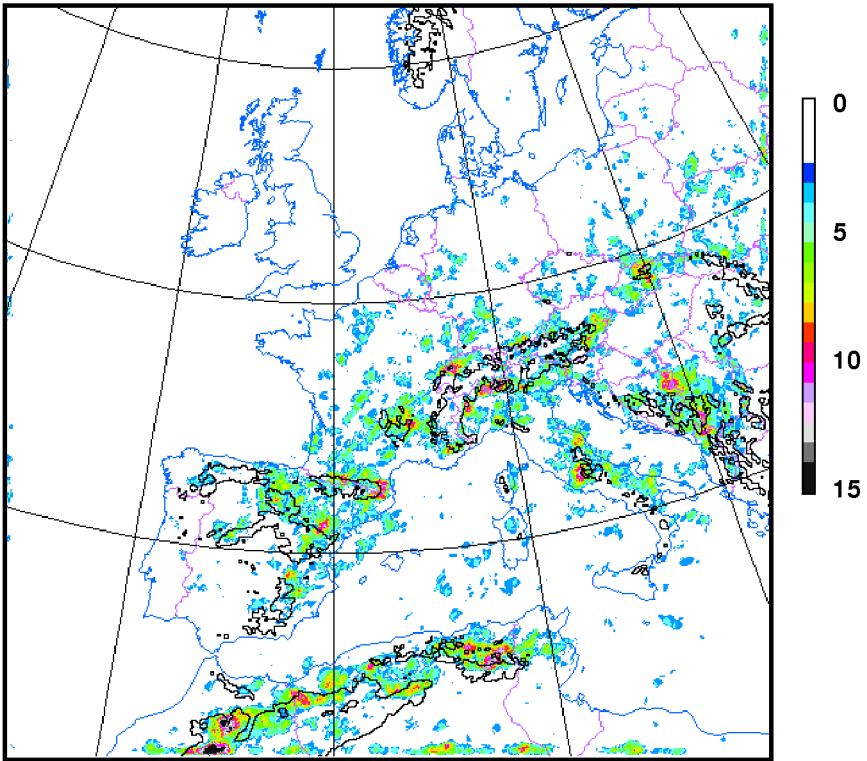


Figure 2. Density map of mesoscale convective systems (MCSs) triggering for the 4813 trajectories beginning normally (in number of MCSs triggering over each pixel). The black solid line is the 1000-metre elevation contour.

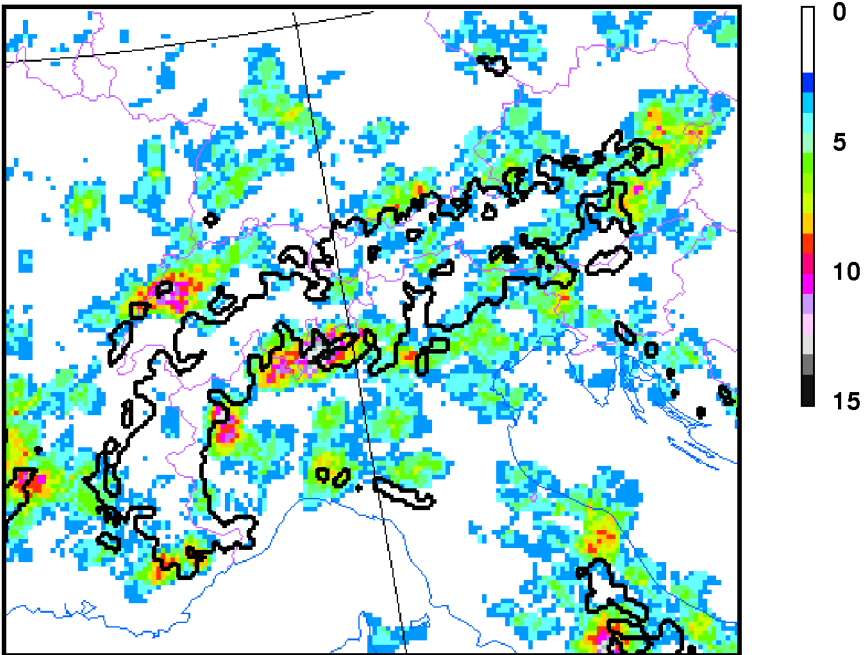


Figure 3. Same as Fig. 2, zoomed over the Alps.

more integrations of systems and 941 (35%) MCSs with three or more splits. This seems to be physically consistent with the mechanism of triggering of convective systems by former ones, which is not balanced by a physically based merging mechanism. Nevertheless, further work would be necessary to study in more depth the phenomena of regeneration and merging of systems.

3. MESOSCALE-CONVECTIVE-SYSTEM GEOGRAPHICAL LOCATION

(a) *Maps of mesoscale-convective-system triggering*

MCS triggering is defined as the first detection time of the cloud system by ISIS (i.e. first time that the system area below -45°C exceeds 1000 km^2). It is assumed that the location of the system at that time is a good approximation of its triggering location given the scale we are working at. In order to obtain smooth density maps of MCS triggering, MCS extent at triggering time is defined as the MCS best-fitting ellipse extent at that time. The grid of these maps is the same as the grid of satellite images.

Figure 2 displays the density map of MCS triggering for the 4813 trajectories beginning normally in the MCS database described in section 2. It shows that MCS triggering is strongly correlated with orography. Indeed, there are maxima of MCS triggering near all of the mountain ranges. Maxima of MCS triggering are observed not only near the largest mountain ranges, like the Alps and the Atlas Mountains, but also near smaller ones (for instance the Pyrenees, the Massif Central, the Jura, the Apennines and the Iberian Mountains). Nevertheless, it must be noted that some MCSs trigger over flat regions (like the north of France, Belgium or north of Germany) far away from any orographic influence.

Another observation is that MCS triggering is rather rare ($\simeq 6\%$) over the Mediterranean during the warm season. A seasonal study (see section 3(c)) of the triggering shows that 53% of the MCSs which trigger over the Mediterranean between March and September occur between 15 August and 30 September. This result is in good agreement with the climatologies concerning Mediterranean convective activity (Tuduri and Ramis 1997) which shows that this activity occurs during the entire autumn with a maximum of activity in October.

The same density map zoomed over the Alps is displayed in Fig. 3. It clearly shows the different areas which favour the MCS triggering near the Alps:

- The Lombard lakes region where a maximum of 18 MCSs (3.6 MCSs per year) is registered over the valley of Como Lake. The Garda Lake region seems to be less active with a maximum of 'only' 10 MCSs (2 per year).
- The eastern part of Jura is also an area of favoured MCS triggering with a maximum of 14 MCSs (2.8 per year) near Neuchatel Lake.
- The regions of the Aoste valley and Torino have a maximum of 13 MCSs (2.6 per year).
- The southern French Alps and the eastern Austrian Alps have a maximum of 11 MCSs (2.2 per year).
- Friuli, the area of München and the area of Genova have a maximum of 10 MCSs (2 per year).

When interpreting these figures, one should bear in mind that what are called MCSs are MCSs triggering 'normally' (i.e. not coming from the regeneration of a pre-existing MCS) and reaching at least an area of $10\,000\text{ km}^2$ at a temperature threshold of -45°C . Note that the MCS frequencies shown in these figures are probably overestimated as false alarms are mainly due to orographic cloud shields, see section 4(b) of part I.

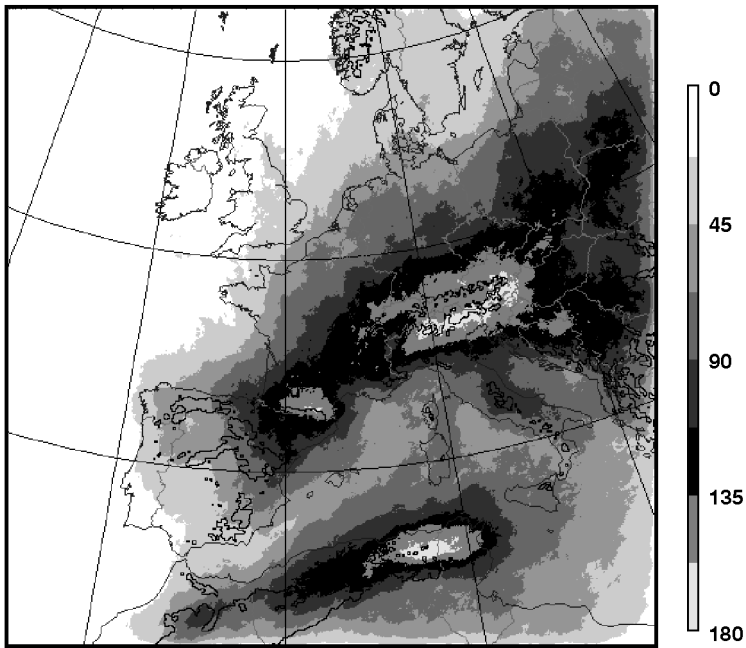


Figure 4. Density map of mesoscale convective system (MCS) occurrences for the whole database (in number of MCS occurrences over each pixel).

(b) *Map of mesoscale-convective-system occurrences*

The map of MCS occurrence density is given in Fig. 4. This includes the whole MCS database (6311 trajectories). The units are in number of MCSs (MCS best-fitting ellipse) which were located over a given pixel at any time of their life cycle. It must be underlined that this map shows the occurrence of MCSs, and not the occurrence of cloud shields of MCSs, meaning that if a given system was located over the same pixel in more than one image, it was counted only once. This map reinforces the conclusions of section 3(a), showing that MCS occurrence is very frequent near mountains, with a maximum of MCS occurrences over the Alps, the Pyrenees and the Atlas Mountains. For instance, a line of around 160 MCS occurrences is observed all along the southern side of the Alps, from the Lombard lakes to the eastern Austrian Alps with a maximum of 176 MCS occurrences over the Lombard lakes region. As already noted, the data in these figures are probably overestimated as false alarms are mainly due to orographic cloud shields.

This map also shows that European MCSs are mainly continental and concern all of Europe. Continental areas with the lower MCS occurrences are Ireland, the United Kingdom and the Scandinavian countries, but also Portugal and the western and southern areas of Spain. The lack of strong diurnal heating during the warm season can explain the low MCS activity over Ireland, the United Kingdom and the Scandinavian countries. For Portugal and Spain, the physical mechanism responsible for the low MCS activity is probably the lack of humidity at low levels, as these regions are very dry during the warm season, and also due to the lack of an efficient triggering source such as a mountain ridge.

Moreover, it shows that there is a narrow band of low MCS occurrence between north-African systems and European systems, extending along the Mediterranean coasts

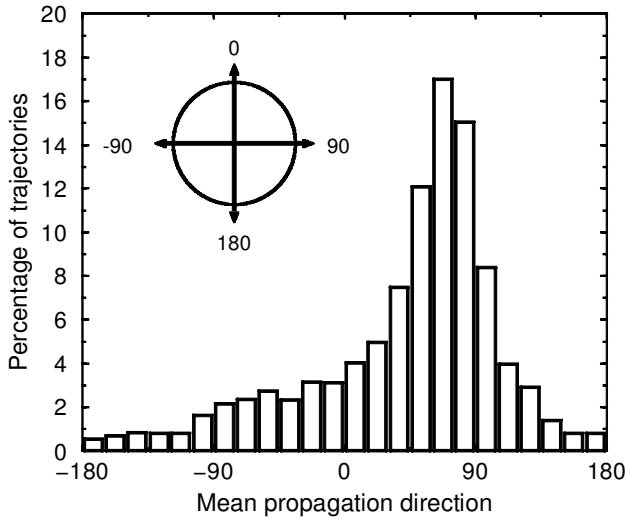


Figure 5. Distribution of the mean propagation direction for the whole database.

of southern Spain from Gibraltar to Corsica and passing through the Balearic Islands (with a small increase in MCS activity over Corsica, Sardinia and the Balearic Islands). This could be explained by the south-westerly mean flow during the warm season and by the lack of important triggering mechanisms over this region.

Finally, the comparison between the density map of MCS triggering (Fig. 2) and this map of MCS occurrence, suggests that most of the systems have an east-north-east motion. For instance, concerning the Alpine MCSs, the maximum of MCS triggering is located in the western part of the southern side of the Alps (Lombard lakes, areas of Torino and Genova) and the maximum of MCS occurrence extends to the eastern part of the southern side of the Alps, from the Lombard lakes to Austria. To confirm this, the distribution of the mean propagation direction, which is the direction between the positions of the first and last detected MCS centres of gravity is displayed in Fig. 5 for the whole MCS sample. It shows that 44.1% of the systems propagate toward the east-north-east (mean propagation direction between 45° and 90°) and that only 5.1% have a southward motion ($< -135^\circ$ and $> 135^\circ$). The propagation direction of MCSs is then in good correspondence with the south-westerly mean mid-level flow and consequently, this supports the concept of the steering level which assumes that the motion of MCSs matches the environmental wind at a given mid-tropospheric level (Hagen *et al.* 1999).

(c) Monthly distributions of mesoscale-convective-system occurrence

In order to characterize the monthly distributions of MCS occurrence during the warm season, the monthly total of the 4813 MCSs beginning normally is plotted in Fig. 6. As already mentioned, the number of MCS occurrences strongly increases during April, then reaches a maximum from May to August, with fewer MCSs during July, and starts to decrease during September. By plotting the monthly number of MCSs for the subset of the MCSs which trigger north of latitude 40°N (3422 trajectories, dashed line in Fig. 6) and for the 843 MCSs which trigger over north Africa (dot-dashed line in Fig. 6), it is possible to explain the relative minimum number of MCSs during July by the rapid fall of MCS occurrence over north Africa during July (224 MCSs in June and only 48 in July, also see the monthly density maps displayed in Fig. 7). The monthly

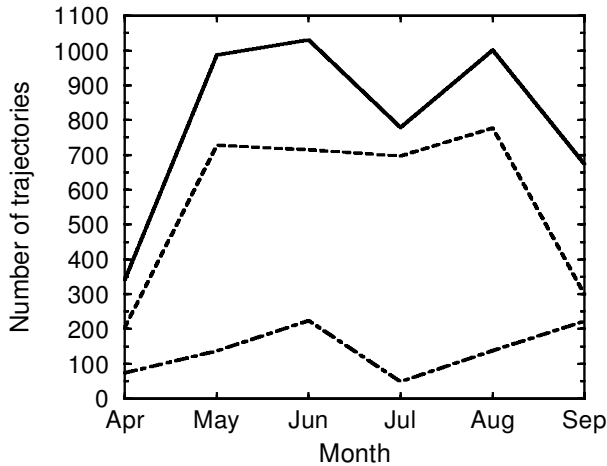


Figure 6. Monthly number of mesoscale convective systems (MCSs): (i) for the 4813 MCSs beginning normally (solid line), (ii) for the subset of this sample composed of MCSs which trigger north of latitude 40°N (dashed line), (iii) for the subset of this sample composed of MCSs which trigger over north Africa (dot-dashed line).

number of European MCSs is thus nearly maximum and constant (in number of MCS triggering) from May to August.

Figure 7 addresses the monthly distributions of European MCSs during the warm season by plotting the monthly density maps of MCS occurrence for the 4813 trajectories beginning normally. The units of these maps are the same as in Fig. 4 (in number of MCSs over each pixel).

The main conclusions are the following:

- In April, few MCSs are observed over a wide part of Europe.
- Then, the number of MCSs increases very quickly in May. There is no well defined region of MCS activity, and in fact, MCSs occur everywhere over land, even far away from the main European mountain ranges. However, regions with a maximum of MCS occurrence are mainly located over eastern Europe: (i) north of the Carpathian Mountains, over Ukraine, Byelorussia and Poland and (ii) north of the western Balkans over Yugoslavia where more than 35 MCS occurrences (7 per year) are registered.
- In June, MCS activity is shifted southward and a maximum of MCS occurrence is located over the south-eastern side of the Alps (Friuli region in Italy and Slovenia) and over Austria with a maximum value of 40 MCS occurrences (8 per year) over the Friuli region. The MCS activity north of the Carpathian Mountains is greatly diminished and far fewer MCSs occur north of latitude 50°N. MCSs in the western Balkans region are still occurring but are shifted to the north-west over Romania and north of Yugoslavia.
- In July, most MCS occurrences are located near the Alps, while the remaining MCS activity observed over Romania in June is rapidly decreasing. The main difference between June and July for the Alpine MCSs is that they occur as frequently on both sides of the Alps. Consequently, MCSs become very frequent in the south of Germany (with more than 30 MCS occurrences, 6 per year, over the whole southern part of Bavaria) and in Switzerland (with a maximum of 40 MCS occurrences, 8 per year, near the German border). The absolute maximum of MCS occurrence is also shifting from the south-eastern side of the Alps to the north-eastern side over the border between Germany and Austria with 43 MCS occurrences (8.6 per year) registered.

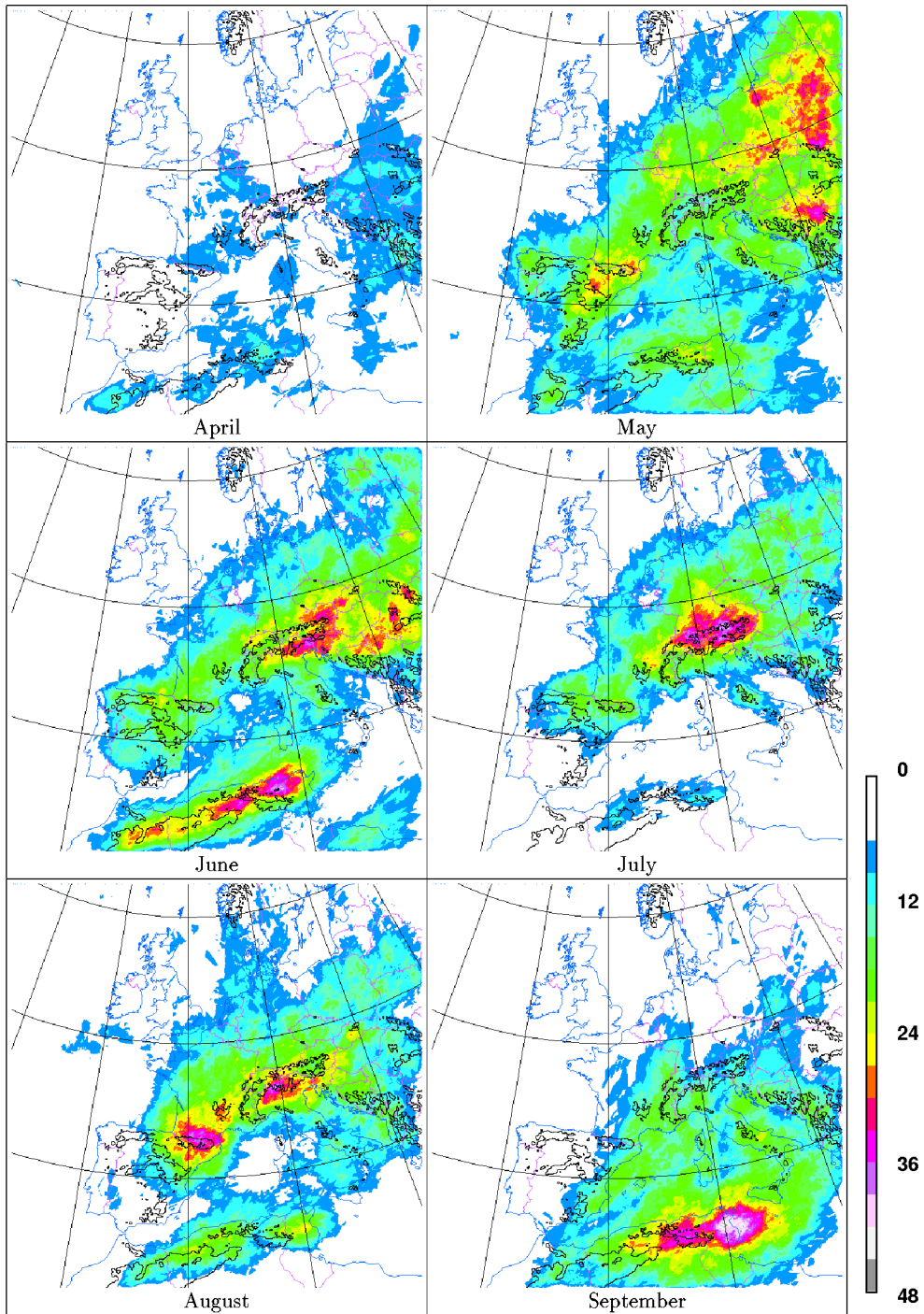


Figure 7. Monthly density maps of mesoscale convective system (MCS) occurrence for the 4813 trajectories beginning normally (in number of MCS occurrences over each pixel).

- In August, there is a south-westward shift of MCS activity and they become frequent over France, mainly in the south-west. A lot of MCSs occur near other mountains such as the Pyrenees (with a maximum of 42 MCS occurrences, 8.2 per year) and the Massif Central (with a maximum of 33 MCS occurrences, 6.6 per year) in France. Concerning MCSs which occur near the Alps, the south-westward shift is also clear with a pronounced decrease over Austria and Germany and a maximum (41 MCS occurrences, 8.2 per year) of activity over the Lombard lakes region in Italy.

- Finally, in September, European MCS activity is ending and a marked decrease in MCS occurrence is observed near the Alps and the Pyrenees. MCS activity greatly increases over the Mediterranean (around 40% of the MCSs that trigger over the Mediterranean between April and September, trigger in September). Also note that the monthly maximum of MCS occurrence is observed during this month in Tunisia with 48 MCS occurrences (9.6 per year).

Some characteristics of the monthly distributions of MCS activity over Europe were already noted by previous authors. For instance:

- The two regions of the Alps (Friuli and the Lombards lakes), where maxima of MCS occurrences are observed, are also evident from precipitation climatologies (e.g. Frei and Schär 1998; Hulme and Conway 1995).

- The maximum of MCS occurrences observed in July near the border between Germany and Switzerland corresponds to a maximum of lightning activity as presented in Finke and Hauf (1996).

- The beginning of MCS activity over the Mediterranean during September is coherent with the climatology of convective events in the western Mediterranean described in Tuduri and Ramis (1997) and Carretero and Riosalido (1996).

4. MORPHOLOGICAL CHARACTERISTICS OF MESOSCALE CONVECTIVE SYSTEMS

(a) *Mesoscale-convective-system maximum-extent distribution*

The distribution of MCS maximum extent is given in Fig. 8 for the *simple* MCS trajectories sample (see section 2). It shows that there is no gap in this distribution: MCSs evenly cover the meso- α scale and part of the meso- β one. It also shows that very large MCSs remain rare in Europe. Indeed, 50.4% of the systems have a maximum extent lower than 20 000 km² and only 5.6% reach an area of 100 000 km² or more. This underlines the need for a sound climatology of European MCSs below the MCC scale.

The search for an analytical form of MCS maximum extent has already been presented by several authors (e.g. Williams and Houze 1987; Augustine *et al.* 1989; Mapes and Houze 1993), who concluded that the accumulated frequency of MCS maximum extent was log-normally distributed (see appendix). Our aim is to study the impact of having a limited observation window (only above an area of 10 000 km²) on the evaluation of the log-normal distribution parameters. Figure 9(a) displays the accumulated frequency of MCS maximum extent for the same *simple* MCS trajectories sample. This accumulated frequency is plotted on a log-probability scale which means that the x -axis is plotted on a logarithmic scale and the y -axis on a normal probability scale. In such a diagram, the curve of a log-normal accumulated frequency is a straight line.

Figure 9(a) shows that the accumulated frequency is very close to a straight line from 30 000 km² up to 200 000 km². According to Lopez (1977), our choice to study only those MCSs reaching 10 000 km² could be responsible for the deviation observed

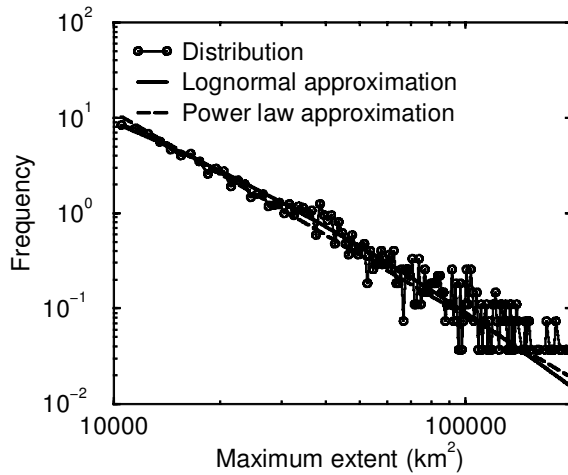


Figure 8. Distribution of mesoscale-convective-system maximum extent. The solid line is a log-normal approximation ($m = 7.85$ and $\sigma = 1.59$), the dashed line is a power-law approximation (slope = -2.14).

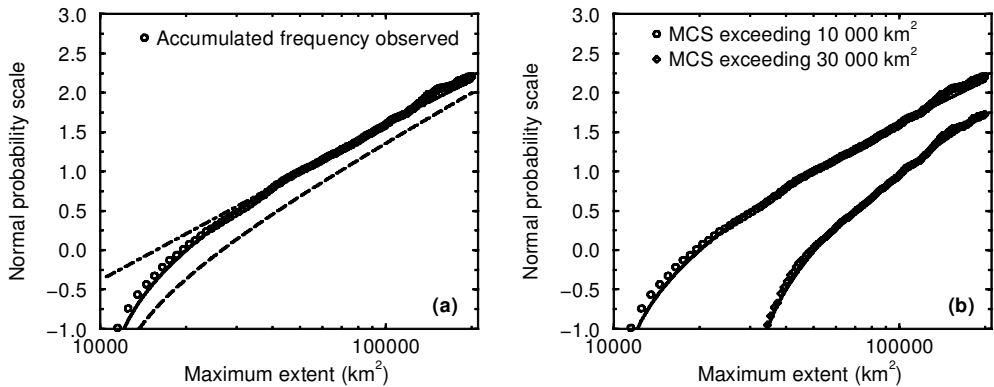


Figure 9. (a) Accumulated frequency of mesoscale convective system (MCS) maximum extent (the dot-dashed line is the log-normal curve evaluated according to a linear regression between $40\,000\text{ km}^2$ and $100\,000\text{ km}^2$, the dashed line is the same log-normal curve truncated at $10\,000\text{ km}^2$, the solid line is the log-normal curve truncated at $10\,000\text{ km}^2$ evaluated according to a maximization of the likelihood). (b) Accumulated frequency of MCS maximum extent for MCSs exceeding $10\,000\text{ km}^2$ (circles) and for MCSs exceeding $30\,000\text{ km}^2$ (squares). The log-normal distributions ($m = 7.85$ and $\sigma = 1.59$) truncated at both $10\,000\text{ km}^2$ and $30\,000\text{ km}^2$ are the solid lines.

between $10\,000\text{ km}^2$ and $30\,000\text{ km}^2$. One way to derive the distribution parameters is to perform a linear regression between $40\,000\text{ km}^2$ and $100\,000\text{ km}^2$. This leads to the parameter values $m = 9.7$ and $\sigma = 1.2$ for the log-normal distribution which best fits the actual distribution over this range of area. This best-fitting log-normal curve is plotted in Fig. 9(a) with a dot-dashed line and is, of course, a straight line. The dashed line in Fig. 9(a) is this best-fitting log-normal curve truncated at $10\,000\text{ km}^2$ (see appendix). It does not fit at all the accumulated frequency of MCS maximum extent, showing that the best-fitting log-normal curve evaluated from a linear regression leads to incorrect values for parameters m and σ .

Using a maximum-likelihood technique (Lindgren 1962), it is possible to evaluate parameters m and σ of a log-normal distribution truncated at $10\,000\text{ km}^2$ that best

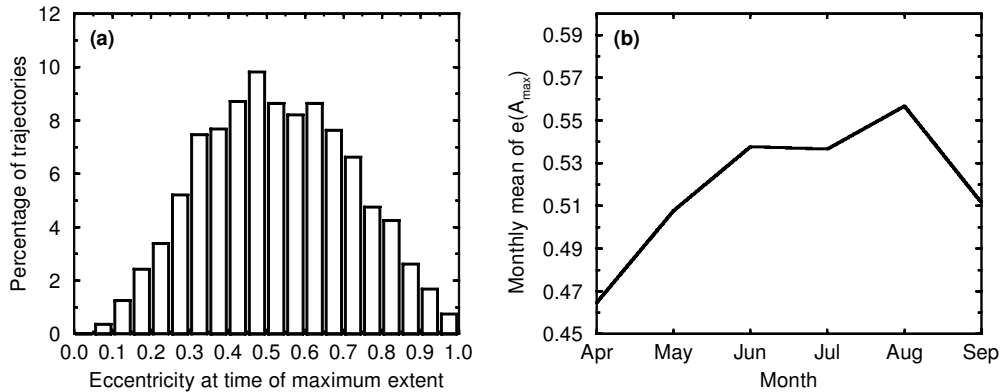


Figure 10. (a) Distribution of mesoscale convective system (MCS) eccentricity at the time of maximum extent. (b) Monthly mean of MCS eccentricity at the time of maximum extent.

fits (in terms of likelihood) the MCS maximum-extent distribution observed. This leads to $m = 7.85$ and $\sigma = 1.59$. The corresponding log-normal distribution is plotted in Fig. 9(a) by a solid line and fits the observed distribution very well. It must be emphasized that this log-normal distribution provides a satisfactory approximation to the MCS maximum-extent distribution whatever the area threshold A_{\min} (greater than $10\,000\text{ km}^2$). For instance, Fig. 9(b) displays the observed accumulated frequency of MCS maximum extent for MCSs exceeding $30\,000\text{ km}^2$ and the log-normal distribution of parameters $m = 7.85$ and $\sigma = 1.59$ truncated at $30\,000\text{ km}^2$. The result shows a very good match.

Other authors have proposed power laws to fit MCS area distributions (e.g. Machado *et al.* 1992). It could be interesting to objectively compare such a law with the proposed log-normal law. In Fig. 8, the observed distribution of MCS maximum extent is compared with the above log-normal distribution (solid line) and with a power law with a slope equal to -2.14 evaluated using the maximum-likelihood technique. These two approximations seem equally satisfactory all along the observed maximum-extent range spectrum. However, only the log-normal approximation is statistically validated by the Kolmogorov–Smirnov test at the 5% significance level (Lindgren 1962), with a test value of 0.018 for a level of significance of 0.026 (the test value for the power law is 0.044).

Using classical formulae for log-normal distributions, it is concluded that the average value of MCS maximum extent is around 9100 km^2 which leads to a typical radius of around 50 km. The standard deviation of MCS maximum-extent distribution is around $30\,000\text{ km}^2$, showing that MCSs cover a wide range of maximum extent.

(b) Mesoscale-convective-system eccentricity at the time of maximum extent

Most climatologies of MCSs concern MCCs, and hence make use of a measure of cloud-shield shape. Figure 10(a) displays the distribution of eccentricity at the time of maximum extent, hereafter called $e(A_{\max})$, for the *simple* MCS trajectories sample. This eccentricity $e(A_{\max})$ is defined as the ratio of the minor axis to the major axis of the MCS best-fitting ellipse at the time of maximum extent. It shows a rather symmetric distribution, with a mean value of 0.53 and values over the whole possible range. Moreover, only 20.6% of the MCSs have an eccentricity at the time of maximum extent greater than 0.7, which is the shape criteria used to define MCCs: this shows that the

majority of European MCSs are not as circular as MCCs. In fact, only 23 MCSs ($\approx 0.8\%$) could qualify as quasi-MCCs having a $e(A_{\max})$ greater than 0.7 and an area at the time of maximum extent greater than $100\,000\text{ km}^2$ at a temperature threshold of $-45\text{ }^\circ\text{C}$.

Figure 10(a) shows also that some European MCSs have a pronounced elongated shape, with 12.6% having an $e(A_{\max})$ value lower than 0.3. This is probably due to the presence of frontal convective systems in the MCS sample. Indeed, from April to May, when frontal convection is important due to frontal spring systems crossing Europe, 16.9% of MCSs have an $e(A_{\max})$ value lower than 0.3 against only 10.4% for summer convective systems starting between June and August. This result is consistent with the observed intra-seasonal trend of the mean monthly value of $e(A_{\max})$ (Fig. 10(b)). This mean grows from 0.46 in April to 0.56 in August and drops back to 0.51 during September. Similar results were observed over the USA by Augustine *et al.* (1989). Reasons for this slight seasonal cycle are not obvious but should involve the scarcity of strong shear during summer (compared with spring and autumn when strong baroclinicity is more frequent). This weaker shear could, therefore, favour the occurrence of more circular systems.

5. DURATION AND DIURNAL CYCLE OF MESOSCALE CONVECTIVE SYSTEMS

In this section, we define the MCS triggering time as the time of first detection of the system, i.e. of the first image in which the system reaches an area of more than 1000 km^2 . In a similar way, the MCS dissipation time is defined as the time of last detection of the system (last image in which the system reaches an area of more than 1000 km^2).

(a) *Mesoscale-convective-system duration*

The MCS duration is defined as the duration between the time of first detection and the time of last detection. The histogram of MCS duration in Fig. 11(a) relates to the *simple* MCS trajectories sample. It shows that the typical value of MCS duration is 5.5 hours with 38% of the MCSs having a duration of between 5 and 8 hours. It also shows that some trajectories in the MCS sample have a very long duration (4.7% above 20 hours), those trajectories are supposed to be due to convective systems embedded in fronts.

Fig. 11(a) also shows that the choice to keep only the trajectories exceeding a minimum area value of $10\,000\text{ km}^2$ in the MCS sample discards MCSs with low durations. Indeed, only 20 trajectories (0.7%) last less than 3 hours. In order to demonstrate that the MCS duration distribution is highly sensitive to the chosen minimum area value of MCSs, Fig 11(b) displays the area at the time of maximum extent versus the duration of MCSs. It shows that the choice to study only MCS trajectories exceeding $10\,000\text{ km}^2$ biased the duration histogram of the whole population of convective events up to around 10 hours (upper limit of MCSs having a maximum extent around $10\,000\text{ km}^2$). Consequently, the above results are strongly correlated with the $10\,000\text{ km}^2$ thresholding; for example, a thresholding at a minimum area value of $20\,000\text{ km}^2$ would have led to the following figures: 8 hours as the typical value of MCS duration and around 2.4% of the MCS population lasting less than 5 hours. To give an analytical form to this distribution is then not of much use, nonetheless it was checked that the histogram of MCS duration fits quite well, given the half-hour accuracy, a log-normal distribution (see Fig. 11(a)).

Figure 11(b) also shows an expected result: the longer an MCS lasts, the bigger it is. However, Fig. 11(b) shows that some MCSs can last very long (more than 10 hours)

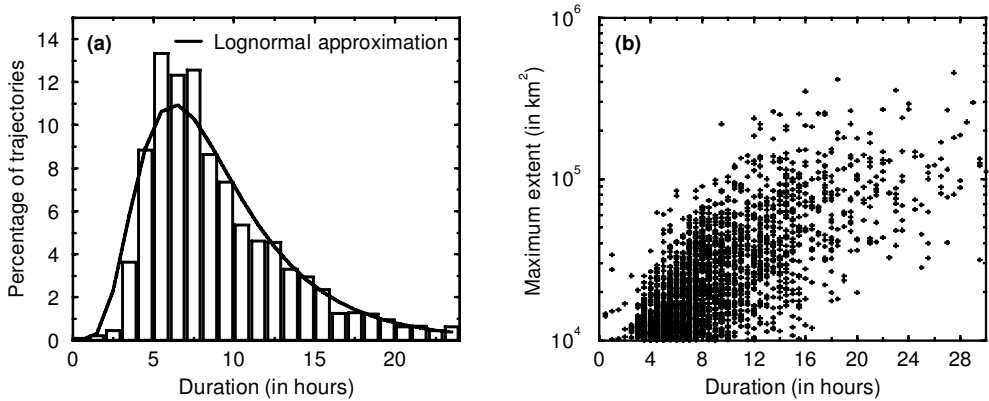


Figure 11. (a) Histogram of mesoscale convective system (MCS) duration and its log-normal approximation (solid line). (b) Area at time of maximum extent versus duration of MCSs.

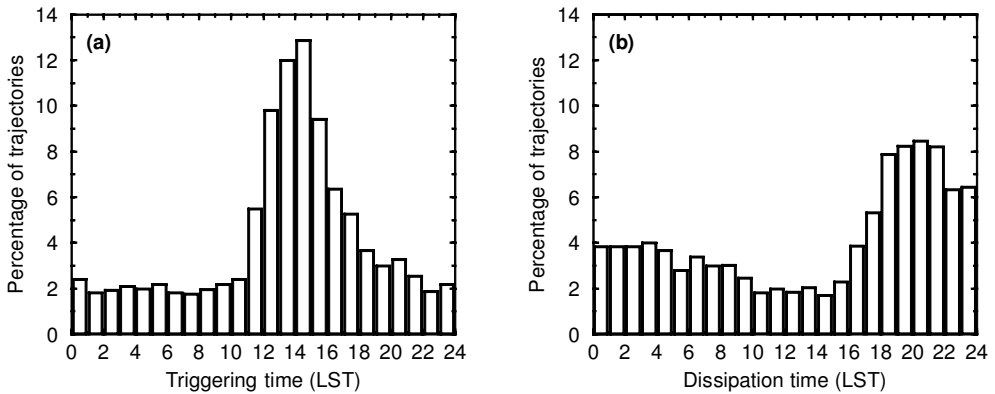


Figure 12. (a) Distribution of the mesoscale convective system (MCS) triggering time. (b) Distribution of dissipation time, in Local Solar Time (LST).

without exceeding 20 000 km². MCS regeneration is probably the dynamical mechanism responsible for such cases because it leads to the development of several consecutive MCSs generated by outflows of previous MCSs, which may be interpreted as a single MCS trajectory by the tracking method.

(b) *Mesoscale-convective-system diurnal cycle*

Figure 12(a) displays the histogram of MCS triggering time for the *simple* MCS trajectories sample. All the times given in this section are Local Solar Time (LST) meaning that it takes into account the longitude of the MCS gravity centre at the time of first (for the triggering time) or last (for the dissipation time) detection.

It shows that the diurnal cycle of MCS triggering is strongly correlated with the diurnal heating of the low levels of the atmosphere. Indeed, a marked peak of MCS triggering is observed during the afternoon. More precisely, this peak starts near 11 a.m., then reaches its maximum around 2 p.m. and decreases up until 9 p.m. Then, during the second part of the night and the morning, the distribution of MCS triggering time remains nearly constant showing that more than 20% of MCS triggering (21.9% start between 10 p.m. and 9 a.m.) is not due to the diurnal heating but to other lifting

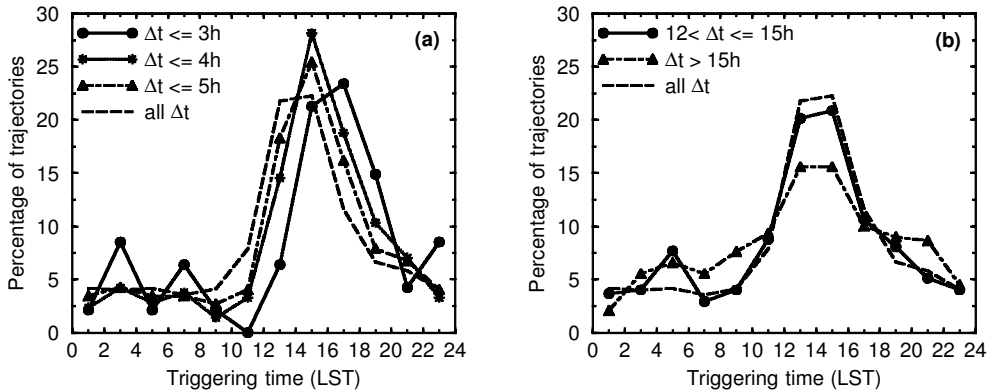


Figure 13. Distribution of the mesoscale convective system (MCS) triggering time for different intervals of MCS duration Δt , in Local Solar Time (LST).

mechanisms (such as frontal forcing, mid-level cold pools or outflows of pre-existing MCSs).

The histogram of MCS dissipation time is presented in Fig. 12(b) for the same MCSs. It also shows a marked diurnal cycle with a peak of MCS dissipation shifted by around 5 hours to the early evening, which is consistent with the typical duration of MCSs.

Distributions of MCS triggering times are displayed in Fig. 13 for different classes of MCS duration (Δt). Figure 13(a) shows results for short durations ($\Delta t \leq 3$ h, $\Delta t \leq 4$ h, and $\Delta t \leq 5$ h). This includes, respectively, 47, 213, and 519 MCSs. By comparing these histograms with the general one, it is observed that the peak of triggering time is shifted toward the end of the afternoon for short duration MCSs, this shift being more and more important when considering MCSs of shorter and shorter duration. This tendency for short-living MCSs to start later in the afternoon than MCSs of long duration is explained by the fact that by starting later in the afternoon when the diurnal heating is decreasing, most of these short-living systems do not have enough time to develop and establish mesoscale circulations which could allow them to last during the evening and the night when instability disappears.

The distributions of MCS triggering time for long-duration MCSs ($12 < \Delta t \leq 15$ h, 273 cases, and $\Delta t > 15$ h, 289 cases) are displayed in Fig. 13(b). The afternoon peak of MCS triggering is less pronounced for MCSs having a very long duration ($\Delta t > 15$ h). This can be explained by the presence of convective systems embedded in fronts for which the triggering is not sensitive to diurnal heating but dominated by dynamical factors.

In the distribution of MCSs lasting between 12 and 15 hours, the diurnal cycle of MCS triggering is well marked and very close to that of the whole sample one, except that a secondary maximum of MCS triggering is observed in the early morning with a peak at 4% around 5 a.m. Easterling and Robinson (1985) also found that the diurnal cycle of storms could show a secondary maximum in the early morning for some places (North Carolina). But, after a visual examination of the MCSs which trigger between 4 and 6 a.m., it is concluded that no region seems to favour their triggering. Finally, this secondary maximum could also be a sampling effect: a peak of 4% in this MCS sample represents around 10 MCS trajectories. This result thus has to be checked over a larger sample.

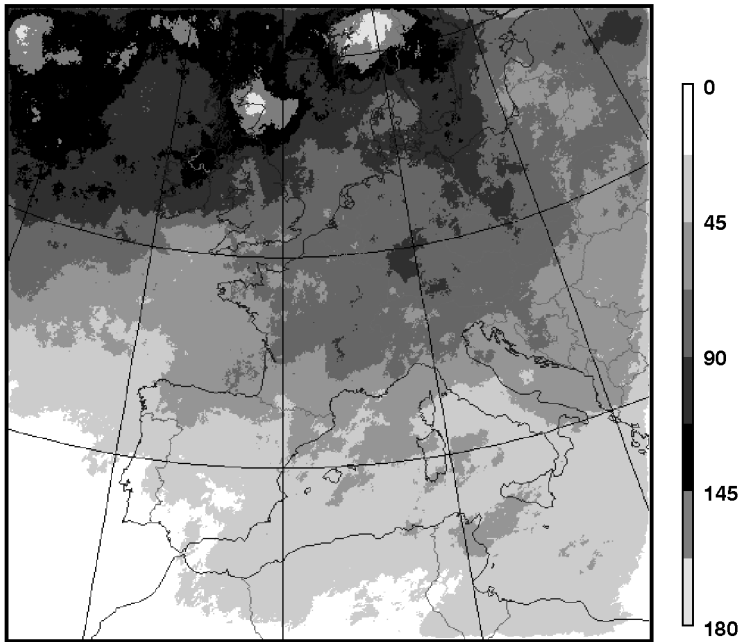


Figure 14. Density map of occurrence for the non-convective sample (in number of system occurrences over each pixel).

6. INDIRECT VERIFICATIONS OF THE DISCRIMINATION METHOD

The goal of this section is to ensure that the method of discrimination between convective and non-convective trajectories, which was validated over France (see section 3 of part I of this paper), is working correctly during the warm season over the whole geographical domain considered. The non-availability of lightning data outside France and the surrounding areas resulted in the need to make some indirect verifications of the usefulness of the method based on the comparison between the convective and non-convective samples.

Hereafter, the convective sample is composed of the previously studied 6311 trajectories which is then the whole sample of trajectories satisfying the MCS discrimination criteria. The non-convective sample is composed of the 7916 trajectories which do not satisfy the MCS discrimination criteria.

The first verification deals with the geographical distribution of non-convective systems. The map of numbers of occurrence for the 7916 non-convective trajectories is shown in Fig. 14 and is similar to Fig. 4, which shows convective cases. It shows that the non-convective activity is collocated with the north-Atlantic storm track during the warm season. Indeed, most of the non-convective system occurrences are located northward of the 50°N latitude with some maxima of non-convective activity in the north-western part of the domain, over Ireland, Scotland and the Scandinavian countries. On the other hand, the occurrence of convective systems (see Fig. 4) is mainly over land and close to mountains where it is known that convection triggering is favoured by diurnal heating of the low levels of the troposphere over land and by orographic lifting. The geographical locations of main activity and maxima in both maps then seem physically sound and this forms the first consistency check for the discrimination method.

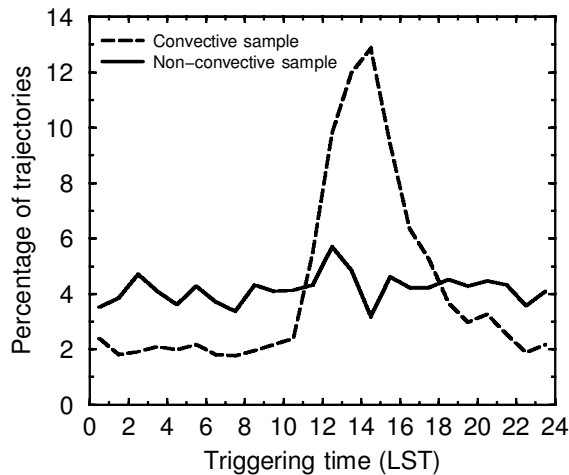


Figure 15. Distribution of the triggering time for 2723 ‘simple’ trajectories of the convective sample (dashed line) and for the 2105 ‘simple’ trajectories of the non-convective sample (solid line), in Local Solar Time (LST).

The second indirect verification makes use of the triggering-time distributions. This study was only performed on ‘simple’ trajectories (i.e. fully described and *over-crossing* MCS trajectories with normal beginnings and endings). As discussed in section 5(b), the distribution of MCS triggering time is marked by a diurnal cycle with a peak during the afternoon caused by radiative heating. The distribution of non-convective system triggering time (Fig. 15) does not show such a diurnal cycle. This is physically consistent with the fact that this sample is mainly composed of frontal systems for which the triggering is not favoured by the diurnal heating. This second indirect verification reinforces the assumption that the discrimination method is applicable to the full geographic domain.

Both verifications are only consistency checks, and do not provide objective probabilities of detection and false-alarm rates. This could be done, provided that lightning data were made available at the European scale with an adequate detection efficiency.

7. CONCLUSION

For the first time, a sound database of European MCSs has been built using Meteosat infrared images and a fully automated method (see part I of this paper). This method has been fully validated over France and its surroundings (see part I) and, thanks to consistency checks on this database (see section 6), seems to be efficient over a large European domain.

The derived climatology of European MCSs covers five warm seasons (between April and September) for the years 1993 to 1997 and covers Europe, the western Mediterranean and northern Africa. It is composed of more than 6000 trajectories of MCSs exceeding, at least once, an area of 10000 km² at a temperature threshold of -45°C .

The main conclusions concerning European MCS geographical distribution are the following:

- European MCSs are mainly continental. Nevertheless, MCSs start to be more frequent over the Mediterranean Sea during the latter part of August and September.

- European MCS triggering is strongly correlated with orography and maxima of MCS triggering are observed near all mountain ranges. The orographic lifting is thus a dominant source of European MCS triggering.

- Alpine MCS triggering is favoured in the following regions: the Lombard lakes, the eastern part of the Jura near the Neuchatel Lake, the areas of the Aoste valley and Torino, the southern French Alps, the eastern Austrian Alps, Friuli, the area of München and the area of Genova.

- A narrow band of low MCS activity is observed off the Mediterranean Spanish and French coasts downstream (in average south-westerly flow) of the Gibraltar Strait.

- The monthly distributions of MCS occurrences have also been detailed. Briefly, it demonstrates that the number of European MCSs is remarkably constant from May to August and that a global south-westward shifting of MCS activity is observed during the warm season: starting in eastern Europe in May, then moving to the south with the first Alpine MCS occurrences in June and MCS activity concerning only the Alps during July. In August, even if there is still some activity near the Alps, many MCSs trigger over the Pyrenees and Spain, and finally, in September, MCS occurrences are mainly located over the Mediterranean Sea and north Africa.

The conclusions concerning the main characteristics of European MCSs are as follows:

- European MCS trajectories are rather complex. Indeed, only around half of the MCSs trigger and end 'normally' (i.e. not during a split or a merge with another cloud system). Moreover, among this 55% of MCS trajectories, most of them split or merge with other cloud systems during their life cycle (only 373 MCSs do not). The need to find an objective way to quantify the complexity of MCS trajectories is thus very important.

- The direction of propagation of MCSs is mainly toward the east-north-east and very few systems have a southward motion. This agrees with the mid-level flow over Europe during the warm season, which is mainly south-westerly.

- European MCSs evenly cover the meso- α scale down to the upper meso- β one. Moreover, around 50% of the studied MCSs do not reach a maximum extent of 20 000 km², showing the need for a climatology of rather small European MCSs.

- The distribution of the MCS maximum extent can be approximated by a log-normal distribution ($m = 7.85$ and $\sigma = 1.59$) leading to an average value of MCS maximum extent of around 9000 km² and a standard deviation of around 30 000 km². This analytical approximation is not dependent upon the choice to study only MCSs reaching at least 10 000 km². The approximation of this distribution by a power law has been statistically rejected.

- The European MCS shape at the time of maximum extent varies from band to quasi-circular shapes. The study of the seasonal cycle of mean MCS eccentricity shows a tendency for summer MCSs to be more circular.

- Around 40% of the MCSs last between 5 and 8 hours and very few MCSs (less than 1%) last less than 3 hours. These two figures are highly linked to the choice to study only systems with areas exceeding, at least once in their lifetime, 10 000 km².

- A diurnal cycle of MCS triggering has been demonstrated and is correlated with the diurnal heating of the atmosphere. Indeed, the MCS triggering-time distribution reveals a marked peak starting near 11 a.m., reaching its maximum near 2 p.m. and decreasing up until 9 p.m. (LST). The same kind of diurnal cycle is observed in terms of the dissipation times, with a peak of MCS dissipation between 7 and 10 p.m. (LST).

- Despite this diurnal cycle, it is observed that around 20% of the MCSs trigger between 10 p.m. and 9 a.m. (LST), showing that diurnal destabilization of the atmosphere is not responsible for all the MCS triggering but that at least one fifth of the MCS triggering is due to other mechanisms, like for instance frontal forcing, cold pools at mid-levels or outflows from other systems.

- Finally, MCSs with short durations tend to trigger later in the afternoon than MCSs with longer durations and the triggering time of MCSs with very long durations is less sensitive to the diurnal heating.

Future work will consist of further exploitation of this database. We have already mentioned the usefulness of an objective method of quantifying the complexity of MCS trajectories. Other features already computed in the existing database are still to be studied, such as the evolution of MCS area at different temperature thresholds. A more detailed study of some types of MCSs, like large or quasi-stationary MCS populations, would no doubt be of interest too. A search for statistical forecasting rules for the duration and maximum extent of MCSs may also be undertaken. For example, correlations between total duration and initial growth rates could be studied.

The database could also be linked with other sources of data. Indeed, this database should be taken as the first, promising milestone leading to a future multi-parametric description of MCSs. The storage of date, location, direction of propagation and best-fitting ellipse parameters makes possible a merge with a wide range of other data. For instance, a study concerning the electrical life cycle of MCSs is already feasible for MCSs occurring over France and the surrounding areas using the integration of lightning data over the trajectories. A merging between these MCSs and radar data, in order to study for example the organization of convective cells below a sole cold anvil, is also manageable. Relationships between MCS occurrence and environmental conditions, as described by analysed fields of numerical weather-prediction models, could be fruitful too. They could allow progress in the understanding of conceptual models of MCSs and help to characterize the environmental situations which are likely to favour and enhance MCS development. And finally, a classification of these MCSs between strongly and weakly precipitating convective systems using high-density daily raingauge network data must be realized in order to better understand the physical mechanisms at hand.

APPENDIX

The log-normal distribution $d(x)$, with parameters m and σ , is defined as the distribution of x when $\ln x$ follows a normal law, and it can be shown to satisfy (e.g. Lindgren 1962):

$$d(x) = 0 \quad \text{if } x \leq 0,$$

$$d(x) = \frac{1}{x\sqrt{2\pi}\sigma} \exp\left(\frac{-(\ln x - m)^2}{2\sigma^2}\right) \quad \text{if } x > 0.$$

A log-normal distribution $d_X(x)$, with parameters m and σ , truncated at X is then defined as:

$$d_X(x) = 0 \quad \text{if } x \leq X,$$

$$d_X(x) = \frac{1}{I(m, \sigma)} \frac{1}{x\sqrt{2\pi}\sigma} \exp\left(\frac{-(\ln x - m)^2}{2\sigma^2}\right) \quad \text{if } x > X,$$

with

$$I(m, \sigma) = \int_X^{+\infty} d(y) dy.$$

REFERENCES

- Anderson, J. C. and Arritt, R. W. 1996 'MCC versus non-MCC mesoscale convective systems: Features associated with initiation'. Pp. 491–493 in preprint volume of the Symposium on mesoscale analysis and forecasting, 9–13 September 1996, Reading, UK
- Arnaud, Y., Desbois, M. and Maizi, J. 1992 Automatic tracking and characterization of convective systems on Meteosat pictures. *J. Appl. Meteorol.*, **31**, 443–453
- Augustine, J. A. and Howard, K. H. 1991 Mesoscale Convective Complexes over the United States during 1986 and 1987. *Mon. Weather Rev.*, **119**, 1575–1589
- Augustine, J. A., Tollerud, E. I. and Jamison, B. D. 1989 'Distributions and other general characteristics of mesoscale convective systems during 1986 as determined from GOES infrared imagery'. Pp. 437–442 in preprint volume of the 12th Conference on weather analysis and forecasting, 2–6 October 1989, Monterey, CA, USA
- Carretero, O. and Riosalido, R. 1996 'Mesoscale Convective Systems—a five-year Meteosat satellite climatology over Spain'. Pp. 185–189 in preprint volume of the 1996 Meteorological satellite data users' conference, 16–20 September 1996, Eumetsat, Vienna, Austria
- Easterling, D. R. and Robinson, P. J. 1985 The diurnal variation of thunderstorm activity in the United States. *J. Clim. Appl. Meteorol.*, **24**, 1048–1058
- Finke, U. and Hauf, T. 1996 The characteristics of lightning occurrence in southern Germany. *Contrib. Atmos. Phys.*, **69**, 361–374
- Frei, C. and Schär, C. 1998 A precipitation climatology of the Alps from high-resolution rain-gauge observations. *Int. J. Climatol.*, **18**, 873–900
- Hagen, M., Bartenschlager, B. and Finke, U. 1999 Motion characteristics of thunderstorms in southern Germany. *Meteorol. Appl.*, **6**, 227–239
- Hodges, K. I. and Thorncroft, C. D. 1997 Distribution and statistics of African convective weather systems based on the ISCCP Meteosat imagery. *Mon. Weather Rev.*, **125**, 2821–2837
- Hulme, M., Conway, D., Jones, P. D., Jinag, T., Barrow, E. M. and Turney, C. 1995 Construction of a 1961–1990 European climatology for climate change modelling and impact applications. *Int. J. Climatol.*, **15**, 1333–1363
- Kane, R. J., Chelius, C. R. and Fritsch, J. M. 1987 Precipitation characteristics of mesoscale convective weather systems. *J. Clim. Appl. Meteorol.*, **26**, 1345–1357
- Laing, A. G. and Fritsch, J. M. 1993a Mesoscale Convective Complexes in Africa. *Mon. Weather Rev.*, **121**, 2254–2263
- 1993b Mesoscale Convective Complexes over the Indian monsoon region. *J. Climate*, **6**, 911–919
- 1997 The global population of Mesoscale Convective Complexes. *Q. J. R. Meteorol. Soc.*, **123**, 389–405
- Lindgren, B. W. 1962 *Statistical Theory*. The Macmillan Company
- Lopez, R. E. 1977 The log-normal distribution and cumulus cloud populations. *Mon. Weather Rev.*, **105**, 865–872
- Machado, L. A. T., Desbois, M. and Duvel, J. P. 1992 Structural characteristics of deep convective systems over tropical Africa and the Atlantic ocean. *Mon. Weather Rev.*, **120**, 392–406
- McAnelly, R. L. and Cotton, W. R. 1989 The precipitation life cycle of Mesoscale Convective Complexes over the central United States. *Mon. Weather Rev.*, **117**, 784–808
- Maddox, R. A. 1980 Mesoscale Convective Complexes. *Bull. Am. Meteorol. Soc.*, **61**, 1374–1387
- Mapes, B. E. and Houze, R. A. 1993 Cloud clusters and superclusters over the oceanic warm pool. *Mon. Weather Rev.*, **121**, 1398–1415
- Mathon, V. and Laurent, H. 2001 Life cycle of the Sahelian mesoscale convective cloud systems. *Q. J. R. Meteorol. Soc.*, **127**, 377–406
- Miller, D. and Fritsch, J. M. 1991 Mesoscale Convective Complexes in the western Pacific region. *Mon. Weather Rev.*, **119**, 2978–2992
- Morel, C. and Senesi, S. 2002 A climatology of mesoscale convective systems over Europe using satellite infrared imagery. I: Methodology. *Q. J. R. Meteorol. Soc.*, **128**, 1953–1971

- Tollerud, E. I., Augustine, J. A. and Jamison, B. D. 1992 'Cloud top characteristics of Mesoscale Convective Systems in 1986'. Pp. J3-J7 in preprint volume of the 6th Conference on satellite meteorology and oceanography, 5-10 January 1992, Am. Meteorol. Soc., Atlanta, USA
- Tuduri, E. and Ramis, C. 1997 The environments of significant convective events in the western mediterranean. *Weather and Forecasting*, **12**, 294-306
- Velasco, I. and Fritsch, J. M. 1987 Mesoscale convective complexes in the Americas. *J. Geophys. Res.*, **92**, 9591-9613
- Williams, M. and Houze Jr., R. A. 1987 Satellite-observed characteristics of winter monsoon cloud clusters. *Mon. Weather Rev.*, **115**, 505-519